Static Dielectric Properties of Carbon Nanotubes from First Principles

Boris Kozinsky[1] and Nicola Marzari[2]

[1]*Department of Physics, MIT, Cambridge, Massachusetts 02139, USA*
[2]*Department of Materials Science and Engineering, MIT, Cambridge, Massachusetts 02139, USA*
(Received 28 September 2005; published 24 April 2006)

We characterize the response of isolated single-wall (SWNT) and multiwall (MWNT) carbon nanotubes and nanotube bundles to static electric fields using first-principles calculations and density-functional theory. The longitudinal polarizability of SWNTs scales as the inverse square of the band gap, while in MWNTs and bundles it is given by the sum of the polarizabilities of the constituent tubes. The transverse polarizability of SWNTs is insensitive to band gaps and chiralities and is proportional to the square of the effective radius; in MWNTs, the outer layers dominate the response. The transverse response is intermediate between metallic and insulating, and a simple electrostatic model based on a scale-invariance relation captures accurately the first-principles results. The dielectric response of non-chiral SWNTs in both directions remains linear up to very high values of applied field.

Carbon nanotubes attract a lot of scientific interest due to their unique and versatile electronic and mechanical properties, suitable for a wide range of applications. Nanotubes have different electronic properties, determined in the zone-folding scheme by the chiral vector: Armchair (m, m) nanotubes are 1D metals, and zigzag $(m, 0)$ nanotubes are semiconductors, with (almost) vanishing gaps for $m = 3n$. Synthesis and separation of specific nanotubes remains a central challenge. Variations in chirality and size influence dielectric properties, which in turn can be exploited for separation; e.g., electric fields have been used to align nanotubes during plasma-enhanced chemical vapor-deposition (PECVD) synthesis [1,2] and to separate different tubes in solutions [3]. A detailed physical understanding of dielectric response is also needed to characterize optical excitations, screening at contacts, plasmons in nanotube arrays, and the degree of control achievable on endohedral fillings. While in recent years the response of single-wall carbon nanotubes (SWNTs) has been studied with tight-binding [4–6] and first-principles approaches [7,8], multiwall carbon nanotubes (MWNTs)—a more common product of synthesis—have received much less attention due to their complexity. We present here a comprehensive and detailed picture of dielectric screening in SWNTs, MWNTs, and bundles, using a combination of first-principles techniques and introducing an accurate classical electrostatic model that captures the unusual response of these materials.

All calculations are performed using QUANTUM-ESPRESSO [9] with the Perdew-Burke-Ernzerhof approximation and ultrasoft pseudopotentials in a plane-wave basis. A tetragonal unit cell is set up with periodic-boundary conditions in 3D and a k-point sampling grid of at least $30 \times 1 \times 1$. Atomic configurations are generated using an interatomic distance of 1.42 Å, obtained from careful relaxation studies [10]. Longitudinal and transverse polarizabilities are calculated using density-functional per-turbation theory (DFPT) [11] and finite-field or electric-enthalpy approaches [12]. Since we use periodic-boundary conditions, we effectively simulate a three-dimensional bulk material consisting of a square array of infinite parallel nanotubes. The longitudinal dielectric response of an isolated nanotube is characterized by the polarizability per unit length $\alpha_\parallel$, which is related to the separation-dependent bulk dielectric constant $\epsilon_\parallel$ via

$$\epsilon_\parallel = 1 + \frac{4\pi}{\Omega} \alpha_\parallel, \qquad (1)$$

where $\Omega = L^2$ is the cross-sectional area of the unit cell. From linear-response theory [13], we expect the static dielectric constant to depend on the gap as $\epsilon(q) \approx 1 + (\hbar\omega_p/\Delta_g)^2$, which suggests via (1) that $\alpha_\parallel \sim 1/\Delta_g^2$. Our calculations confirm this behavior in zigzag nanotubes, as shown in Fig. 1. As expected, $(9, 0)$, $(12, 0)$, and $(15, 0)$ nanotubes have the smallest gaps and the largest $\alpha_\parallel$; the inverse-square dependence on the gap roughly holds over 2 orders of magnitude. Only the narrowest nanotubes $(7, 0)$ and $(8, 0)$ deviate from this trend. The agreement is particularly accurate for large-gap zigzag nanotubes $(3n + 1, 0)$ and $(3n + 2, 0)$, with $n > 2$. We note in passing that for these SWNTs our first-principles results can be fitted well with these relations: $\Delta_g \approx 3.3/R_0 + 0.06$ and $\alpha_\parallel \approx 8.2R_0^2 + 20.5$, with Δ_g in eV and R_0 in Å. Previous tight-binding studies [4] reported values of $\alpha_\parallel$ comparable to ours and noted a relation $\alpha_\parallel \sim R_0/\Delta_g^2$, which we also observe for large-gap nanotubes (Fig. 1). For infinitely long armchair SWNTs, the longitudinal polarizability per unit length $\alpha_\parallel$ diverges since there is no gap in the band dispersions. To get a sense of scaling, we can approximate such nanotubes as metallic ellipsoids of length l and transverse radius R ($l \gg R$); the classical result is $\alpha_\parallel \sim l^2/[24(\ln(l/R) - 1)]$. For MWNTs, the longitudinal picture remains simple: Depolarization effects along the axis
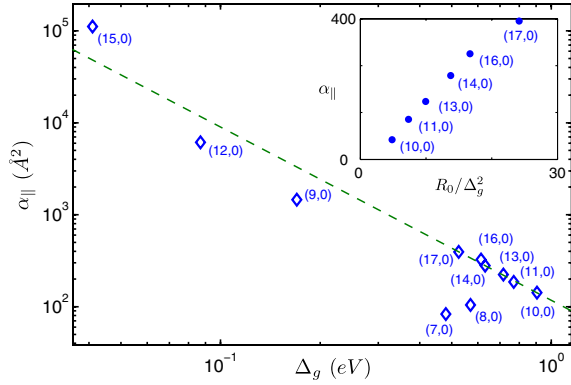
FIG. 1 (color online).   Log-log plot of $\alpha_\parallel$ of zigzag SWNTs as a function of band gap. The dashed line has slope -2. The inset shows $\alpha_\parallel$ for large-gap SWNTs as a function of R_0/Δ_g^2.

are negligible, and constituent tubes have very weak dielectric interactions. The total polarizability $\alpha_\parallel^{\text{tot}}$ should then be the sum of polarizabilities of constituent SWNTs; this conclusion is confirmed by our results in Table I.

We address the characterization of the transverse dielectric response in two different ways. First, we calculate with DFPT the dielectric constant $\epsilon_\perp$, from which the transverse polarizability $\alpha_\perp$ is extracted. To study nonlinear finite-field effects, we also obtain $\alpha_\perp$ by applying an electric field E_{out} via a sawtooth potential and computing the total induced dipole moment per unit length $p_\perp$. In the linear regime, the two approaches are equivalent, and we find an

TABLE I.   Radius of the carbon backbone, band gap, and transverse and longitudinal polarizabilities (per unit length) of carbon nanotubes as a function of the chiral vector (n, m).

(n, m)	R_0 (Å)	Δ_g (eV)	$\alpha_\perp$ (Å^2)	$\alpha_\parallel$ (Å^2)
$(7, 0)$	2.74	0.48	6.47	83.0
$(8, 0)$	3.15	0.57	7.80	104
$(9, 0)$	3.58	0.17	9.32	1460
$(10, 0)$	3.95	0.91	10.9	142
$(11, 0)$	4.34	0.77	12.7	186
$(12, 0)$	4.73	0.087	14.3	6140
$(13, 0)$	5.09	0.72	16.3	224
$(14, 0)$	5.48	0.63	18.4	279
$(15, 0)$	5.88	0.041	20.3	11 100
$(16, 0)$	6.27	0.61	22.9	326
$(17, 0)$	6.66	0.53	25.2	395
$(8, 0) + (17, 0)$	$\cdots$	$\cdots$	25.8	499
$(8, 0) + (16, 0)$	$\cdots$	$\cdots$	23.6	427
$(4, 4)$	2.71	(0)	6.41	(∞)
$(5, 5)$	3.40	$\cdots$	8.71	$\cdots$
$(6, 6)$	4.10	$\cdots$	11.6	$\cdots$
$(7, 7)$	4.76	$\cdots$	14.7	$\cdots$
$(8, 8)$	5.45	$\cdots$	18.1	$\cdots$
$(9, 9)$	6.12	$\cdots$	21.8	$\cdots$
$(10, 10)$	6.78	$\cdots$	26.1	$\cdots$
$(12, 12)$	8.14	$\cdots$	35.8	$\cdots$
$(14, 14)$	9.50	$\cdots$	47.2	$\cdots$

agreement between the two methods within 1%. Both DFT-based calculations take into account the local-field effects that would be absent in tight-binding calculations. Again, since calculations provide us with the transverse response of a periodically repeated array of nanotubes, it is necessary to remove the depolarization fields stemming from the periodic images. In principle, one could use

$$\alpha_\perp^b = \frac{\Omega}{4\pi}(\epsilon_\perp - 1) = \frac{p_\perp}{E_{\text{out}}} \qquad (2)$$

for the first and second methods, respectively, while taking the limit $L \to \infty$ for which the depolarization fields vanish. In practice, these persist for very large intertube separations due to the long range of electrostatic interactions between image tubes. Computation time grows as L^2 at a fixed energy cutoff, quickly becoming unmanageable without even reaching a converged result; Fig. 2 illustrates the slowness of this convergence. It is clear, however, that at large separations only electrostatic effects are important, so we can solve this problem using a classical 2D Clausius-Mossotti correction [14] relating the single-tube polarizability $\alpha_\perp$ to the periodic bulk L-dependent value $\alpha_\perp^b$. The relevant conversions are

$$\alpha_\perp = \frac{\Omega}{2\pi} \frac{\epsilon_\perp - 1}{\epsilon_\perp + 1} = \frac{\alpha_\perp^b}{1 + \frac{2\pi}{\Omega}\alpha_\perp^b}. \qquad (3)$$

The values of $\alpha_\perp$ obtained from (3) are listed in Table I and plotted in Fig. 3 as a function of the square of the effective outer radius $\tilde{R} = R_0 + 1.3$ Å (see below). Remarkably, transverse polarizabilities of both metallic and semiconducting SWNTs lie on the same curve, which can be fitted by a line $\alpha_\perp = c\tilde{R}^2$, with slope $c = 0.40$. Thus, chirality and longitudinal band structure have a negligible effect on the transverse dielectric response; this was observed in earlier calculations [4,7,8] and justified with symmetry arguments in the single-particle approximation [4]. Recent tight-binding calculations [5,6] predict a small difference between polarizabilities of metallic and semiconducting SWNTs; however, we do not detect these differences in our DFT calculations.

Periodic-boundary conditions allow us to examine the bulk dielectric response of nanotube bundles. We compute
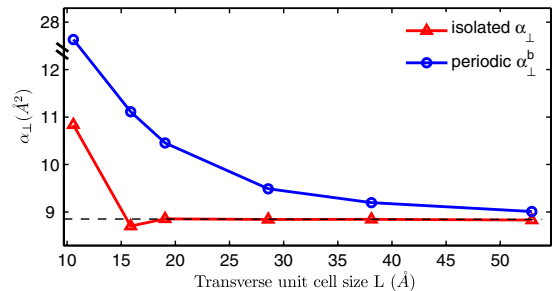

FIG. 2 (color online).   Convergence of $\alpha_\perp$ and $\alpha_\perp^b$ with respect to the size L of the tetragonal unit cell for a $(5, 5)$ SWNT. The point at $L = 10.6$ Å corresponds to a typical tube-tube separation in a nanotube bundle.
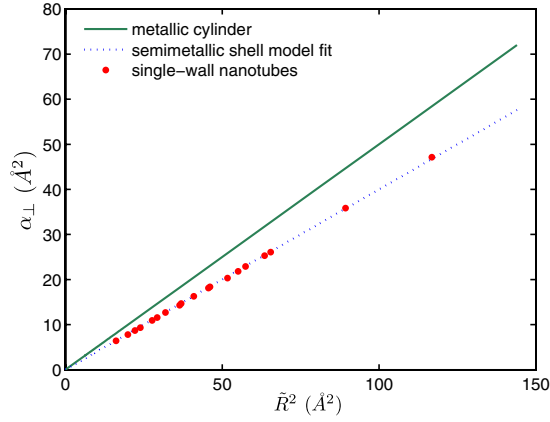
FIG. 3 (color online).   Transverse polarizabilities $\alpha_\perp$ of armchair and zigzag nanotubes as a function of $\tilde{R}^2$. The dashed line is the best-fit result of our semimetallic shell model; the solid line $\alpha_\perp = \frac{1}{2}\tilde{R}^2$ corresponds to an ideal metallic cylinder.

FIG. 4 (color online).   Electrostatic potential for a $(10, 10)$ SWNT in an applied homogeneous transverse field E_{out}. The electric field through the center slice is shown in the inset.

$\epsilon_\perp$ and $\epsilon_\parallel$ of triangular and square arrays with an intertube separation of $d = 3.4$ Å [15]. The values of $\epsilon_\parallel$ accurately match those computed from $\alpha_\parallel$ of isolated nanotubes using (1), thus reflecting the additive property of the longitudinal response. In contrast, the transverse response of bundles depends strongly on d. Figure 2 illustrates both the benefits of using the Clausius-Mossotti relation (3) for large d and the limitation of its applicability when d is small. Whereas the longitudinal response remains simple, the transverse dielectric tensor at small d may have sizable anisotropic and off-diagonal contributions depending on the point-group symmetries of the nanotubes and the lattice. These contributions vanish quickly with d and do not affect our isolated tube calculations.

By applying a finite transverse field E_{out}, we can also study screening inside a nanotube; we find the inner field E_{in} to be very uniform, as shown in Fig. 4. Another remarkable feature is that the screening factor $E_{\mathrm{out}}/E_{\mathrm{in}} \approx 4.4 \pm 0.1$ turns out to be independent of radius and chirality for all SWNTs. To make physical sense of these general results, we look for a simple electrostatic model that would capture these traits. A solid dielectric cylinder of radius $\tilde{R}$ and bulk dielectric constant ϵ would have polarizability $\alpha_\perp = \frac{1}{2}\frac{\epsilon-1}{\epsilon+1}\tilde{R}^2$, a uniform inner field, and a screening factor $E_{\mathrm{out}}/E_{\mathrm{in}} = (\epsilon + 1)/2$ independent of radius. This picture, however, does not correspond to a nanotube, where screening is accomplished by a thin layer of delocalized π electrons. One could then treat a nanotube as a dielectric cylindrical shell of finite thickness. In this case, the inner field remains uniform, but the screening factor decreases with increasing radius. To identify an appropriate model that incorporates all the observed features, we note that, in general, a radius-independent uniform inner field is produced by the surface charge density $\sigma(\phi) = \sigma_0 \cos(\phi)$, where ϕ is the angle measured from the direction of E_{out}. The dipole moment per unit length in this case is $p_\perp = \pi\sigma_0\tilde{R}^2 = \alpha_\perp E_{\mathrm{out}}$ and the polarizability is $\alpha_\perp = (\pi\sigma_0/E_{\mathrm{out}})\tilde{R}^2 = c\tilde{R}^2$, with $c \leq 1/2$. In a metallic cylinder,
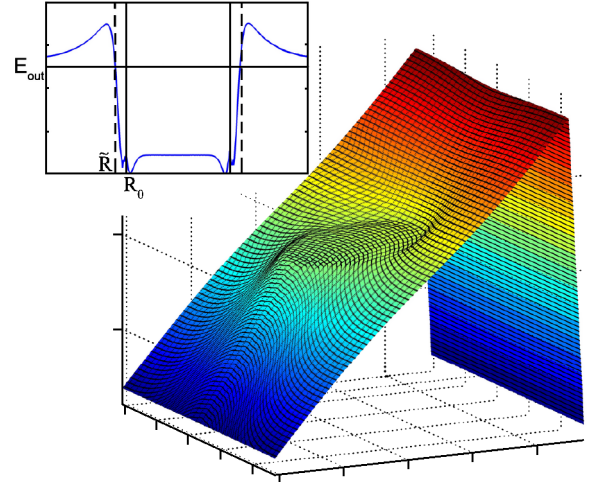
c is $1/2$ and the outer field is completely screened. A best fit of our *ab initio* data for SWNTs to this model (see Fig. 3) yields the slope $c = 0.40$ and effective radius $\tilde{R} = R_0 + 1.3$ Å larger than the radius of the carbon backbone R_0, consistent with the finite thickness of the electronic charge density distribution. Elementary electrostatic considerations yield a screening factor $E_{\mathrm{out}}/E_{\mathrm{in}} = \frac{1}{1-2c} = 5$ in good agreement with our finite-field calculations and previous estimates [4,5]. It should be stressed that the screening properties of nanotubes, reflected in this model, are *neither* metallic nor insulating. This peculiarity is physically grounded in the fact that in a single sheet of graphite the screening of Coulomb interactions is anomalous due to the vanishing density of states at the Fermi points [16]. For carbon nanotubes (as opposed to boron-nitride nanotubes), the semimetallic nature of π electrons implies that the screening factor is radius-invariant.

The generalization of this model to the multiwall case needs to take into account screening and electrostatic interactions between layers. Our strategy is to first solve exactly the general problem of N concentric dielectric cylindrical shells in a uniform field. We then recover precisely the above single-layer model by treating a SWNT as a shell of radius $\tilde{R}$, dielectric constant ϵ, and vanishing thickness δ and constraining these parameters by the scale-invariance condition

$$\epsilon\frac{\delta}{\tilde{R}} = \frac{4c}{1-2c} = \mathrm{const} \qquad (4)$$

that guarantees that the screening factor remains independent of $\tilde{R}$. Modeling a general MWNT amounts to solving a linear system of $2N \times 2N$ boundary-condition equations [17] containing the best-fit parameters c and $\tilde{R}$ (carried over from the single-wall case) and subject to constraint (4). For the double- and triple-wall cases, we find excellent agreement between this model and our *ab initio* results

TABLE II.   Transverse polarizabilities of MWNTs.

MWNT	$\alpha_\perp$ (Å^2) (*ab initio*)	$\alpha_\perp$ (Å^2) (model)
$(8, 0) + (17, 0)$	25.8	25.7
$(5, 5) + (10, 10)$	26.8	26.6
$(4, 4) + (12, 12)$	36.1	36.0
$(9, 9) + (14, 14)$	49.0	48.2
$(4, 4) + (9, 9) + (14, 14)$	49.1	48.3

(Table II). We conclude that the present semimetallic shell model captures all characteristics of the transverse dielectric response: uniform inner field, radius-independent screening factor in SWNTs, and correct $\alpha_\perp$ for MWNTs. We note also that the largest contributions to transverse polarizabilities come from the outer few layers, and inner layers play a negligible role due to screening and their smaller radii. Diameter control alone thus becomes the key growth-parameter determining transverse response.

The finite-field approach is also used to determine the range of fields for which the transverse dielectric response is linear. The $(5, 5)$ nanotube exhibits a precisely linear response with the same polarizability coefficient to within 3 significant digits for fields of 0.05, 0.5, and 5 V/nm. This implies that our electrostatic shell model of transverse response remains valid for large applied fields. To study the linearity of longitudinal response, we minimize the electric-enthalpy functional [12] to introduce a finite longitudinal field in periodic-boundary conditions. We find that the longitudinal response of the $(8, 0)$ nanotube becomes nonlinear by only 5% at $E_\parallel = 0.5$ V/nm. Nonlinearity is, in fact, suppressed because zigzag and armchair (nonchiral) nanotubes are center-symmetric, so the first hyperpolarizability β vanishes by symmetry [7]. To estimate the second hyperpolarizability $\gamma_\parallel$, we compute polarizations at several values of the field and fit the result to the expression $P = \alpha_\parallel E + \gamma_\parallel E^3$. We obtain $\alpha_\parallel = 106$ Å^2 (in agreement with the DFPT result in Table I) and $\gamma_\parallel = 3.1 \times 10^7$ in atomic units.

We now turn to the question of alignment of nanotubes in a uniform electric field. The torque on a nanotube of length l at an angle θ to the field $\mathbf{E}$ is

$$\tau = |\mathbf{p} \times \mathbf{E}| = l(\alpha_\parallel - \alpha_\perp)E^2 \sin\theta \cos\theta. \qquad (5)$$

The longitudinal and transverse polarizabilities compete with each other, but our results imply that $\alpha_\parallel > \alpha_\perp$ in all nanotubes, much more so in metallic and small-gap semiconducting nanotubes. Indeed, for all nanotubes $\alpha_\perp < \frac{1}{2}\tilde{R}^2$, whereas for large-gap SWNTs $\alpha_\parallel \gtrsim 8.2 R_0^2$, and for MWNTs $\alpha_\parallel$ is additive while $\alpha_\perp$ is not. So all nanotubes will align with the electric field, but, by tuning the value of the field during PECVD growth, it may be possible to selectively grow highly polarizable (e.g., metallic) tubes.

There have also been attempts to separate semiconducting and metallic nanotubes in solution using inhomogeneous electric fields [3]. A polarized nanotube aligned with the field will be pulled in the direction of or against the field gradient, depending on its effective dielectric constant $\epsilon_\parallel$ relative to that of the solvent ϵ_s. Assuming no solvent inside the nanotube, and approximating it by a solid dielectric cylinder of radius R_0, we obtain from our values of $\alpha_\parallel$ an effective $\epsilon_\parallel = 1 + 4\alpha_\parallel/R_0^2 \approx 30$ for large-gap semiconducting SWNTs and obviously much larger values for small-gap and metallic tubes. This result is consistent with findings that only metallic SWNTs are observed deposited on the electrodes in water ($\epsilon_s = 80$), whereas all nanotubes are drawn towards the electrodes in isopropyl alcohol ($\epsilon_s = 18$).

In summary, we studied in detail the dielectric properties of isolated and bundled SWNTs and MWNTs. In SWNTs, the longitudinal response is controlled by the band gap, while the transverse response is sensitive only to the effective radius. In bundles and MWNTs, longitudinal response is additive, while the transverse response in MWNTs is dominated by the outer few layers. We presented an accurate scale-invariant electrostatic model of transverse response, which is intermediate between that of a metal and an insulator.

[1] Y. Zhang *et al.*, Appl. Phys. Lett. **79**, 3155 (2001); A. Ural *et al.*, Appl. Phys. Lett. **81**, 3464 (2002).
[2] J. Yu *et al.*, J. Vac. Sci. Technol. B **19**, 671 (2001).
[3] R. Krupke *et al.*, Science **301**, 344 (2003); J. Li *et al.*, Appl. Phys. Lett. **86**, 153116 (2005).
[4] L. X. Benedict, S. G. Louie, and M. L. Cohen, Phys. Rev. B **52**, 8541 (1995).
[5] D. S. Novikov and L. S. Levitov, Phys. Rev. Lett. **96**, 036402 (2006).
[6] Y. Li, S. V. Rotkin, and U. Ravaioli, Nano Lett. **3**, 183 (2003).
[7] G. Y. Guo *et al.*, Phys. Rev. B **69**, 205416 (2004).
[8] E. N. Brothers *et al.*, Phys. Rev. B **72**, 033402 (2005); J. Chem. Phys. **124**, 041101 (2006).
[9] S. Baroni *et al.*, http://www.quantum-espresso.org.
[10] N. Mounet, M.Sc. thesis, MIT, 2005; N. Mounet and N. Marzari, Phys. Rev. B **71**, 205214 (2005).
[11] S. Baroni *et al.*, Rev. Mod. Phys. **73**, 515 (2001).
[12] I. Souza, J. Iniguez, and D. Vanderbilt, Phys. Rev. Lett. **89**, 117602 (2002); P. Umari and A. Pasquarello, *ibid.* **89**, 157602 (2002).
[13] D. R. Penn, Phys. Rev. **128**, 2093 (1962).
[14] F. J. Garcia-Vidal, J. M. Pitarke, and J. B. Pendry, Phys. Rev. Lett. **78**, 4289 (1997); L. Wirtz *et al.*, Phys. Rev. B **71**, 241402(R) (2005); J. Tobik and A. Dal Corso, J. Chem. Phys. **120**, 9934 (2004).
[15] S. Agnihotri *et al.*, Langmuir **21**, 896 (2005); M. F. Lin, Phys. Rev. B **62**, 13 153 (2000).
[16] J. Gonzalez *et al.*, Nucl. Phys. **B424**, 595 (1994); Phys. Rev. B **63**, 134421 (2001).
[17] MATLAB file http://quasiamore.mit.edu/CNT/dielec.html.